Bandpass NGD TAN of Symmetric H-Tree With Resistorless Lumped-Network

Blaise Ravelo, Fayu Wan, Jamel Nebhen, George Chan, Wenceslas Rahajandraibe, Sebastien Lallechere

IEEE Access
Multidisciplinary ⋮ Rapid Review ⋮ Open Access Journal

Received February 19, 2021, accepted March 9, 2021, date of publication March 12, 2021, date of current version March 19, 2021.

Digital Object Identifier 10.1109/ACCESS.2021.3065828

Bandpass NGD TAN of Symmetric H-Tree With Resistorless Lumped-Network

BLAISE RAVELO[1], (Member, IEEE), FAYU WAN[1], (Member, IEEE), JAMEL NEBHEN[2], (Member, IEEE), GEORGE CHAN[3], (Senior Member, IEEE), WENCESLAS RAHAJANDRAIBE[4], (Member, IEEE), AND SÉBASTIEN LALLÉCHÈRE[5], (Member, IEEE)

[1]School of Electronic and Information Engineering, Nanjing University of Information Science and Technology, Nanjing 210044, China
[2]College of Computer Engineering and Sciences, Prince Sattam bin Abdulaziz University, Alkharj 11942, Saudi Arabia
[3]ASM Pacific Technology Ltd., Hong Kong
[4]Institute of Materials, Microelectronics and Nanoscience Laboratory of Provence, UMR7334, CNRS, University of Toulon, Aix-Marseille University, 13397 Marseille, France
[5]SIGMA, Institut Pascal, Université Clermont Auvergne, 63000 Clermont, France

Corresponding author: Sébastien Lalléchère (sebastien.lallechere@uca.fr)

This work was supported in part by the NSFC under Grant 61971230, in part by the Jiangsu Specially Appointed Professor Program and Six Major Talents Summit of Jiangsu Province under Grant 2019-DZXX-022, in part by the Startup Foundation for Introducing Talent of Nanjing University of Information Science and Technology, in part by the Postgraduate Research & Practice Innovation Program of Jiangsu Province under Grant KYCX20_0966, and in part by the Deanship of Scientific Research at Prince Sattam bin Abdulaziz University, Saudi Arabia.

ABSTRACT This paper introduces an innovative passive topology of bandpass (BP) negative group delay (NGD) electrical circuit implemented with symmetric H-tree network. The multi-port topology of BP NGD circuit is originally represented by a resistorless H-tree constituted by lumped LC-passive network. Until now, the NGD electronic circuits available in the literature are implemented by two-port circuits which are using either resistive elements or distributed microstrip topologies. In the present investigation, the feasibility of the modelling, design, fabrication and test of unfamiliar BP NGD original H-tree circuits. The main objective of the study is to identify analytically the existence of the BP NGD function with the resistorless H-tree circuit. Because of its simplicity and the analytical equation compactness, the uncommon approach of tensorial analysis of networks (TAN) is used in the paper. After the branch and mesh analyses, the impedance matrix of the resistorless H-tree is elaborated. Hence, the resistorless H-tree equivalent S-matrix is established by means of impedance to scattering matrix transform. The BP NGD analysis in function of the inductance and capacitance parameters constituting the H-tree circuit is presented. Then, the main steps of the BP NGD investigation are described. The existence of BP NGD behavior in function of the adequate transmission parameters is identified by the consideration of the canonical form. To validate the BP NGD behavior, a proof of concept (POC) of LC-network based resistorless and symmetrical tree prototype is designed, fabricated and measured. Comparison results between well-correlated TAN calculation, simulation and experimentation are discussed.

INDEX TERMS Tensorial analysis of networks (TAN), Kron's formalism, bandpass negative group delay (NGD), resistorless topology, lumped H-tree, symmetric multi-port circuit, S-parameter modeling, LC-network passive circuit.

I. INTRODUCTION

The group delay (GD) effect is susceptible to penalize the communication delay system in addition to the noise effect [1]. This particular parameter can play an important role for the enhancement of signal processing [2]. More unfamiliar function related to the GD attracted the attention of electronic circuit and system engineers when it presents a negative sign [3]–[17].

Thanks to the negative GD (NGD) function, an equalization and compensation of GD and signal delay were introduced [3]–[4]. However, the NGD function remains one of the most unfamiliar electronic function for the research design engineers. Therefore, progressive studies were being

The associate editor coordinating the review of this manuscript and approving it for publication was Dušan Grujić.

conducted by few research teams around the world about the design of the NGD circuits [3]–[15]. Transitively, the meaning of NGD effect was basically highlighted with time domain experimentations [5]–[11]. It was observed that the NGD function enables to propagate a smoothed signal with rise and failing edge in time advance equal to the NGD value [5]–[11]. This counterintuitive function does not contradict the causality principle [5], [6]. Various families of electronic and microwave circuits based on lumped RC and RLC components [12], [13] and metamaterial left-handed structures [14], [15] exhibiting NGD effect were designed. It was pointed out that the time-advance effect related to the NGD effect present a certain time limit [16]. Therefore, simpler approach of NGD analysis was necessary for the non-specialist further familiarity. An analogy between the filter theory and NGD function with the introduction of low-pass and bandpass NGD concept was initiated [17]. But, until now, the existing topologies of NGD lumped circuit are limited to two-port system using resistance elements. In the present study, we are targeting to overcome this NGD circuit theory limited to two-port into a multi-port structure as symmetric H-tree. Before the NGD investigation, it would be necessary to describe a brief state of the art on the H-tree interconnect structures.

The H-tree topology was regularized and deployed by the electronic circuit designers for the electronic and optical signal distributions [18]–[24]. The H-tree interconnects [20]–[24] enable to share certain signals as clock distribution with beneficial simplicity of synchronization. Moreover, further tree topologies [25]–[29] were also introduced for data distribution of different devices as multiphase clock multiplexer, DACs with arbitrary number of levels and clock tree routers. However, the modelling of tree structures against the delay constraints [27], [28] remains an open challenge for the electronic circuit design engineers. Therefore, further modelling methodology related to the tree topology responses prediction must be developed. One of the less deployed ways of the tree interconnect modelling was suggested recently in [29] by considering the tensorial analysis networks (TAN).

We would like to exploit this TAN approach for investigating the possibility to predict the NGD function with H-tree topology in the present paper. In the other words, the present study is double-side original on the identification of innovative H-tree topology exhibiting NGD effect and the TAN modelling. In difference to the existing works on the NGD circuit design which are limited to two-port topology [3]–[17], in the best of the authors' knowledge, a first study on NGD topology implemented with multi-port system is developed in the present paper. As a rigorous method, the analytical approach of the NGD H-tree topology will be developed via the unfamiliar TAN formalism based on the Kron's method [29]–[36].

In brief, the TAN approach was initiated in 1930s for the analysis of electrical machines [30]. This unfamiliar TAN formalism was exploited [31]–[35] to solve electromagnetic compatibility problem of electronic and electrical complex systems. More recently, the potential of TAN formalism became an opportunity to develop, with fast and accurate analytical modelling methods, star tree interconnect lines [29]. The TAN method was also exploited to develop S-parameter model of multi-port system as coaxial cable networks in very few calculation steps [36].

In the present paper, an innovative modelling of NGD analysis for an H-tree lumped circuit topology is investigated. The main novelties of the paper are itemed as follows:

- So far, the research work accomplished on the NGD circuit design are strictly limited to two-port topologies 5]–[17], [37]. The shortcoming of the NGD topology study is the focus on the two-port aspect. However, no research work is currently available on NGD four-port topology. In the best of the authors' knowledge, a first study on NGD topology implemented with four-port circuit is developed in the present paper.
- In addition to the previous point, the NGD electronic circuits available in the literature were implemented by two-port resistive lumped element circuits or distributed microstrip topologies [5]–[17], [37]. In difference to the performed study, the considered NGD four-port topology is constituted by resistorless and symmetric H-tree composed by LC-passive network.
- Then, the S-parameter modelling of the NGD H-tree topology is based on the analytical approach by means of the unfamiliar TAN formalism corresponding to the Kron's method.

The circuit is representing a four-port symmetric structure. To study the BP NGD behavior of the innovative lumped H-tree topology, the paper is mainly organized in five different sections:

- Section II is focused on the S-matrix modelling of the lumped H-tree topology by means of the unfamiliar TAN formalism. The H-tree topology is originally constituted by a resistorless LC-network. The methodology of TAN formalism for the analysis of multi-port topology represented by a symmetric H-tree is described.
- Section III is defining the analysis methodology of an BP NGD ideal response. The main specifications allowing to identify a BP NGD function are recalled.
- Section IV identifies originally one of the H-tree transmission coefficients as an unfamiliar bandpass NGD function characterization for. The basic specifications of the bandpass NGD function are presented.
- Section V is focused on the innovative validation results. A resistorless and symmetric H-tree circuit proof of concept consisted of LC network will be described. Comparison between simulation and measurement of the GD and S-parameter responses will be discussed.
- Then, Section VI is the final conclusion.

II. S-MATRIX MODELLING OF THE SYMMETRIC LUMPED H-TREE WITH TAN FORMALISM

This section describes the S-matrix modelling methodology of the considered multi-port topology. The TAN methodology will be introduced. The different steps of the modelling will be developed for the extraction of the S-matrix model of the lumped H-tree.

A. METHODOLOGY OF TAN MODELLING

To treat an electrical problem of lumped H-tree circuit, the TAN formalism can be described by the following steps:

- Step 1: It consists on the problem formulation by defining the electric circuit representing the multi-port topology by indicating the unknown branch currents.
- Step 2: This step is focused on the graph translation of the circuit defined in the previous step. The topological parameters must be identified in order to classify the sizes of the tensorial variables necessary for the modelling.
- Step 3: The branch space analysis should constitute this step which consists in the description of the branch voltage, the branch current and the branch impedance of the graph established in Step 2.
- Step 4: The mesh space analysis is necessary to reduce the size of the problem defined in the branch space. The mesh voltage, mesh current and mesh impedance are expressed in this step.
- Step 5: The metric of the tensorial problem must be written in this step. The main unknown are the mesh currents. The solution of the problem may be formulated at this stage in function of the problem complexity.
- Step 6: The impedance or admittance matrix can be extracted in this step from the mesh impedance.
- Step 7: The S-matrix model of the multi-port topology can be expressed in this step by means of the impedance of admittance matrix.
- Step 8: The NGD analysis can be realized in the final step, which must be preceded by the phase and GD formulations.

The work flow of Fig. 1 summarizes the methodology of the TAN approach applied to the H-tree modelling. It is constituted by successive phases integrating the different steps previously described.

The application of these steps for the resistorless octopole modelling will be explored in the next subsection.

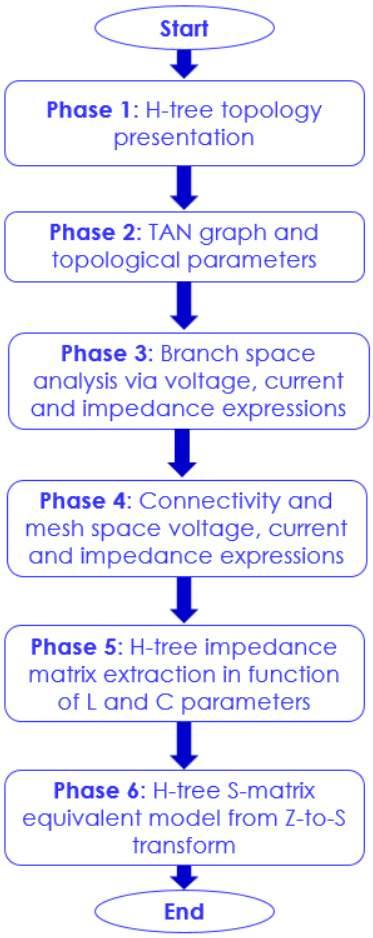

FIGURE 1. Work flow illustrating the different phases of the TAN approach.

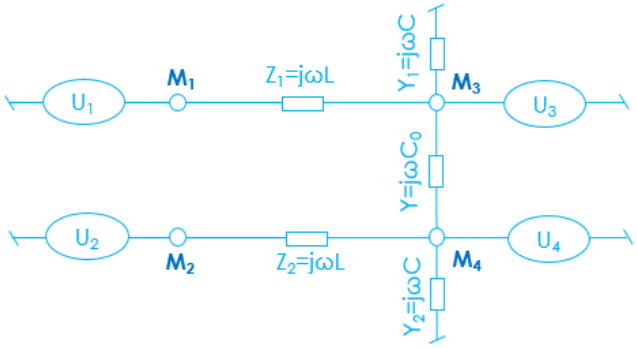

FIGURE 2. Topology of the resistorless and symmetric lumped-network H-tree under study.

B. TAN MODELLING OF RESISTORLESS AND SYMMETRIC LUMPED H-TREE

The H-tree problem will be formulated in the following paragraph. The unfamiliar TAN will be focused on a typical four-port system.

1) STEP1: TOPOLOGICAL INTRODUCTION

The four-port topology represented by H-tree circuit is represented as a symmetric topology shown in Fig. 2. The voltage sources are connected at port, k via node M_k with $k = 1, 2, 3, 4$. The analytical representation of this tree topology will be elaborated with TAN formalism.

The analytical modelling of this H-tree topology depends on the identification of constituting elementary element equivalent impedance or admittances. The circuit is excited by the electrical voltage sources $U_{k=1,2,3,4}$ connected at access port k.

The considered topology is constituted by identical series inductor $L_k = L$ connected in the parallel branches between nodes M_1M_3 and nodes M_2M_4 which presents the impedance:

$$Z_{k=1,2}(j\omega) = Z(j\omega) = j\omega L. \quad (1)$$

A coupling capacitor C_0 connects the nodes M_3M_4 which presents the admittance:

$$Y_c(j\omega) = j\omega C_0 \quad (2)$$

and shunt capacitor $C_{k=1,2} = C$ connecting the nodes M_3 to ground, and M_4 to ground which presents the admittance:

$$Y_{k=1,2}(j\omega) = Y(j\omega) = j\omega C. \quad (3)$$

2) STEP2: TAN GRAPH REPRESENTATION AND TOPOLOGICAL PARAMETRIZATION

The TAN graph equivalent to the H-tree topology introduced in Fig. 2 is drawn in Fig. 3. The topological parameters of the established TAN represented by the numbers of branch, nodes, mesh and port, is addressed in Table 1.

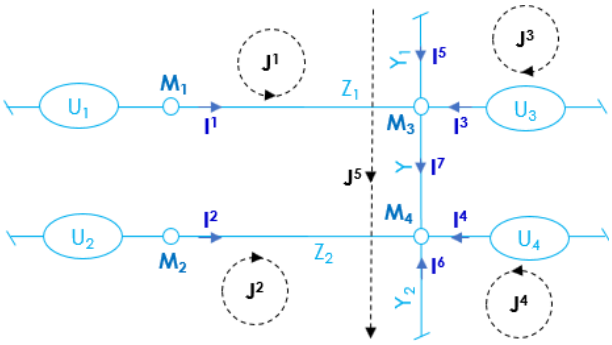

FIGURE 3. TAN graph equivalent of topology introduced in Fig. 2.

TABLE 1. Topological parameters of the graph introduced in Fig. 3.

Parameter	Branch	Node	Mesh	Port	Network
Value	B=7	N=3	M=5	P=4	N_w=1

By denoting the angular frequency variable, ω, the number of ports suggests that four-dimension S-matrix is necessary to model this topology:

$$S_k^m(j\omega) = \begin{bmatrix} S_1^1(j\omega) & S_2^1(j\omega) & S_3^1(j\omega) & S_4^1(j\omega) \\ S_1^2(j\omega) & S_2^2(j\omega) & S_3^2(j\omega) & S_4^2(j\omega) \\ S_1^3(j\omega) & S_2^3(j\omega) & S_3^3(j\omega) & S_4^3(j\omega) \\ S_1^4(j\omega) & S_2^4(j\omega) & S_3^4(j\omega) & S_4^4(j\omega) \end{bmatrix}. \quad (4)$$

3) STEP3: BRANCH SPACE ANALYSIS

The branch space covariant voltage and contravariant current of this H-tree topology can be written as, respectively (a, b =1,2,…,7):

$$V_a(j\omega) = \begin{bmatrix} V_1(j\omega) & V_2(j\omega) & V_3(j\omega) & V_4(j\omega) & 0 & 0 & 0 \end{bmatrix} \quad (5)$$

$$I^b(j\omega) = \begin{bmatrix} I^1(j\omega) \\ I^2(j\omega) \\ I^3(j\omega) \\ I^4(j\omega) \\ I^5(j\omega) \\ I^6(j\omega) \\ I^7(j\omega) \end{bmatrix}. \quad (6)$$

These key variables are linked to the twice covariant branch impedance written in equation (7).

$$\Sigma_{ab}(j\omega) = \begin{bmatrix} Z(j\omega) & 0 & 0 & 0 & 0 & 0 & 0 \\ 0 & Z(j\omega) & 0 & 0 & 0 & 0 & 0 \\ 0 & 0 & 0 & 0 & 0 & 0 & 0 \\ 0 & 0 & 0 & 0 & 0 & 0 & 0 \\ 0 & 0 & 0 & 0 & \frac{1}{Y(j\omega)} & 0 & 0 \\ 0 & 0 & 0 & 0 & 0 & \frac{1}{Y(j\omega)} & 0 \\ 0 & 0 & 0 & 0 & 0 & 0 & \frac{1}{Y_c(j\omega)} \end{bmatrix} \quad (7)$$

4) STEP4: MESH SPACE ANALYSIS

The mesh space covariant voltage and contravariant current of the Y-tree can be written as, respectively ($q, r = 1, 2, \ldots, 5$):

$$X_q(j\omega) = \begin{bmatrix} X_1(j\omega) & X_2(j\omega) & X_3(j\omega) & X_4(j\omega) & X_5(j\omega) \end{bmatrix} \quad (8)$$

$$J^r(j\omega) = \begin{bmatrix} J^1(j\omega) \\ J^2(j\omega) \\ J^3(j\omega) \\ J^4(j\omega) \\ J^5(j\omega) \end{bmatrix}. \quad (9)$$

In order to determine these mesh space variables (voltage, current, impedance) from the branch space ones, we need the proceed with the adequate relationship. The quantity designated connectivity matrix constitutes the adequate solution allowing to determine the mesh variables. Emphatically, the branch to mesh connectivity of graph shown in Fig. 3 is given by:

$$C_r^b = \begin{bmatrix} 1 & 0 & 0 & 0 & 0 \\ 0 & 1 & 0 & 0 & 0 \\ 0 & 0 & 1 & 0 & 0 \\ 0 & 0 & 0 & 1 & 0 \\ 1 & 0 & -1 & 0 & 1 \\ 0 & 1 & 0 & -1 & -1 \\ 0 & 0 & 0 & 0 & 1 \end{bmatrix}. \quad (10)$$

The mesh impedance of the H-tree topology derived from two-rank tensors (8) and (11) is given in equation (11)

with:

$$\Gamma_{km}(j\omega)=\begin{bmatrix} Z_1(j\omega) & 0 & \frac{1}{Y(j\omega)} & 0 & \frac{-1}{Y(j\omega)} \\ 0 & Z_1(j\omega) & 0 & \frac{1}{Y(j\omega)} & \frac{1}{Y(j\omega)} \\ \frac{1}{Y(j\omega)} & 0 & \frac{1}{Y(j\omega)} & 0 & \frac{-1}{Y(j\omega)} \\ 0 & \frac{1}{Y(j\omega)} & 0 & \frac{1}{Y(j\omega)} & \frac{1}{Y(j\omega)} \\ \frac{-1}{Y(j\omega)} & \frac{1}{Y(j\omega)} & \frac{-1}{Y(j\omega)} & \frac{2}{Y(j\omega)} & Z_c(j\omega) \end{bmatrix} \tag{11}$$

$$Z_1(j\omega)=Z(j\omega)+\frac{1}{Y(j\omega)}. \tag{12}$$

5) STEP5: IMPEDANCE MATRIX EXTRACTION

By proceeding similar to the impedance matrix extraction introduced in [37], we can determine the Z-matrix of our topology. We denote the Laplace variable, $s = j\omega$. and the indices, $\{q, r\} = 1, \ldots, 4$. Accordingly, the H-tree topology impedance matrix extracted from previous expression (11) is written as:

$$\Omega_{qr}(s)=\frac{\begin{bmatrix} W(s) & Y_c(s) & Y_t(s) & Y_c(s) \\ Y_c(s) & W(s) & Y_c(s) & Y_t(s) \\ Y_t(s) & Y_c(s) & Y_t(s) & Y_c(s) \\ Y_c(s) & Y_t(s) & Y_c(s) & Y_t(s) \end{bmatrix}}{D_\Omega(s)} \tag{13}$$

with:

$$\begin{cases} Y_t(s)=Y(s)+Y_c(s) \\ W(s)=Y(s)\left[1+\left[2Y_c(s)+Y(s)\right]Z(s)\right]+2Y_c(s) \\ D_\Omega(s)=Y(s)\left[Y(s)+2Y_c(s)\right] \end{cases} \tag{14}$$

6) STEP6: S-MATRIX CALCULATION

With the Z-to-S matrix transform, the S-matrix extraction was performed via the relationship [36]:

$$S_s^q(s)=\left[\Omega_{st}(s)-\Xi_{st}\right]\times\left[\Omega_{qt}(s)+\Xi_{qt}\right]^{-1} \tag{15}$$

by denoting R_0 =50 Ω, the general reference impedance of access ports can be written as:

$$\Xi_{st}=\begin{bmatrix} R_0 & 0 & 0 & 0 \\ 0 & R_0 & 0 & 0 \\ 0 & 0 & R_0 & 0 \\ 0 & 0 & 0 & R_0 \end{bmatrix}. \tag{16}$$

Because of symmetry, we remind that the P-size square S-matrix:

$$S_s^q(s)=\begin{bmatrix} S_1^1(s) & S_1^2(s) & S_1^3(s) & S_1^3(s) \\ S_1^2(s) & S_2^2(s) & S_1^3(s) & S_1^3(s) \\ S_1^3(s) & S_1^3(s) & S_3^3(s) & S_4^3(s) \\ S_1^3(s) & S_1^3(s) & S_3^4(s) & S_3^3(s) \end{bmatrix}. \tag{17}$$

Subsequently, the targeted S-matrix of the symmetric H-tree under study can be calculated from equations (13) and (15).

7) STEP7: NGD ANALYSIS

At the beginning of NGD analysis, it would be important to define the condition between the parameters of the circuit or system topology under study where the NGD behavior can exist and also the associated reflection and transmission coefficients, $S_k^k(j\omega)$, and $S_k^m(j\omega)$, respectively.

By denoting Re(z) and Im(z) the real and imaginary parts of complex number, z, the magnitude of the S-matrix elements is written as:

$$S_k^m(\omega)=\left|S_k^m(j\omega)\right|=\frac{\sqrt{\mathrm{Re}\left\{num\left[S_k^m(j\omega)\right]\right\}^2+\mathrm{Im}\left\{num\left[S_k^m(j\omega)\right]\right\}^2}}{\sqrt{\mathrm{Re}\left\{den\left[S_k^m(j\omega)\right]\right\}^2+\mathrm{Im}\left\{den\left[S_k^m(j\omega)\right]\right\}^2}} \tag{18}$$

with:

$$\begin{cases} num\left[S_k^m(j\omega)\right]=numerator\left[S_k^m(j\omega)\right] \\ den\left[S_k^m(j\omega)\right]=deno\,\mathrm{min}\,ator\left[S_k^m(j\omega)\right] \end{cases}. \tag{19}$$

The GD is one of the less deployed key parameters for evaluating the enveloped signal delay propagating from any port k to any other port m of a given multi-port system. In the present study, our main interest is focused on the case where $k \neq m$. In other words, we would like to express the GD from transmission coefficients, $S_k^m(j\omega)$. The angular phase associated to these transmission coefficients are defined by:

$$\varphi_k^m(\omega)=Arg\left[S_k^m(j\omega)\right]=\mathrm{Arctan}\left\{\frac{\mathrm{Im}\left[S_k^m(j\omega)\right]}{\mathrm{Re}\left[S_k^m(j\omega)\right]}\right\}. \tag{20}$$

The corresponding GD of signal propagating from port k to port m is given by the equation:

$$GD_k^m(\omega)=-\frac{\partial\varphi_k^m(\omega)}{\partial\omega}. \tag{21}$$

The detailed NGD analysis of the resistorless octopole from the previous transmission coefficient will be established in the following section.

III. BP NGD ANALYSIS OF RESISTORLESS AND SYMMETRIC H-TREE

The present section introduces the general specifications of NGD function. The basic analytical equations from the S-matrix established in the previous TAN approach will be exploited.

A. BP NGD FUNCTION SPECIFICATION

Once the GD expression in equation (21) is defined, the NGD analysis can be started with following steps.

1) STEP1: NGD EXISTENCE CONDITION

The initial step consists in proving the existence of NGD which can be analytically formulated by the inequation with unknown the interval of ω:

$$GD(\omega)<0. \tag{22}$$

If this condition is not satisfied, it means that we are facing to completely positive group delay (PGD) system as the cases of classical RC- and LC-filters. Then, the conclusion can be made and it is not necessary to continue the next steps.

2) STEP2: NGD VALUE

This step consists in the identification of NGD center angular frequencies ω_o where the NGD can reach its minimal negative value. If there is a frequency band where the GD can be negative, it would be important to identify the NGD center angular frequencies ω_o where the NGD can reach its minimal negative value:

$$GD_{\min} = GD(\omega_o) < 0. \tag{23}$$

For the case of $\omega_o = 0$, the system is classified as low-pass NGD function. The mathematical equation is not always mathematically easy to solve especially for the case of electrical system constituted by distributed and non-linear topologies. Even if we place under the case of linear circuit constituted only by lumped R, L and C elements, the expressions of GD are usually constituted by polynomial equations with at least degree two. To avoid the mathematical roadblocks, the NGD engineer can proceed with any numerical solvers and also proceed by intuition for the case of complex topologies.

3) STEP3: NGD BANDWIDTH

Fig. 4 represents the GD ideal response of BP NGD function. The NGD center frequency is denoted ω_o whereas the NGD cut-off frequencies are $\omega_{a,b}$, which are the roots of equation:

$$GD(\omega) = 0. \tag{24}$$

As seen in Fig. 4, we take, for example, $\omega_a < \omega_b$. The NGD bandwidth can be determined by the relation:

$$\Delta\omega_{NGD} = \omega_b - \omega_a. \tag{25}$$

The GD is ideally specified by:

$$\begin{cases} GD(\omega < \omega_a) > 0 \\ GD(\omega_a < \omega < \omega_b) < 0 \\ GD(\omega_b < \omega) > 0 \end{cases} \tag{26}$$

In addition to the GD, the levels of reflection and transmission coefficients must be assessed.

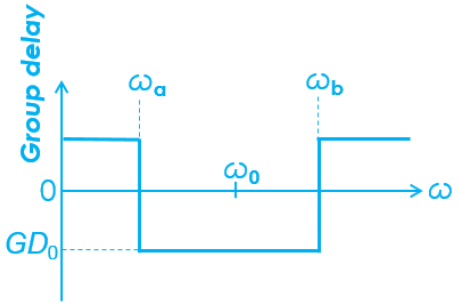

FIGURE 4. Ideal response of BP NGD function.

4) STEP4: REFLECTION AND TRANSMISSION COEFFICIENTS

At this stage of NGD analysis, it is necessary to come back to the S-parameter investigation. Fig. 4 represents ideal specifications of the unfamiliar BP NGD response. Inside the NGD bandwidth, attention must be paid on the transmission coefficient which should not too much attenuated. For example, we can denote the attenuation limit, A, according to the targeted field of applications. Subsequently, the NGD loss can be formulated with the following condition:

$$\left|S_k^m(j\omega)\right| = \left|S_k^m(j\omega)\right|_{\min} > A. \tag{27}$$

It is interesting to note because of Kramer-Koenig theorem, that mostly for the linear circuits we have simultaneously:

$$\tau_{\min} = GD(\omega_o) < 0 \tag{28}$$

$$\left|S_k^m(j\omega)\right|_{\min} = \left|S_k^m(j\omega_o)\right|. \tag{29}$$

The inverse condition must be checked if the targeted application system is sensitive to access mismatching. The reflection coefficient must satisfy the following condition for a given maximal reflection limit B (mostly fixed at -10 dB according to RF and microwave engineering standards):

$$\left|S_k^m(j\omega)\right| = \left|S_k^m(j\omega)\right|_{\min} < B. \tag{30}$$

B. BP NGD INVESTIGATION VIA THE IDENTIFICATION OF CANONICAL FORM

The BP NGD analysis of the resistorless H-tree can be performed by considering the canonical form.

1) ELEMENTARY RESPONSE FOR THE BP NGD ANALYSIS

To identify analytically the BP NGD function of the H-tree topology, we can consider the general case of the transmission coefficient represented as a transfer function (TF):

$$T(j\omega) = S_k^m(j\omega). \tag{31}$$

Therefore, for sake of simplification, because of tree multi-symmetric behavior, for $k \neq m$, all the transmission phases are identical:

$$\varphi(\omega) = \varphi_k^m(\omega) \tag{32}$$

$$GD(\omega) = GD_k^m(\omega). \tag{33}$$

The identification can be made by the determination of the mathematical parameters as defined in the following paragraphs.

2) CANONICAL FORM

The canonical form of elementary BP NGD TF is defined by the second order polynomial formula [37]:

$$T(s) = \frac{s^2 + \omega_\eta s + \omega_0^2}{s^2 + \omega_\psi s + \omega_0^2} \tag{34}$$

with the characteristic parameters, NGD center frequency, ω_0, and also the transmittance attenuation, A, and the GD, τ_0, by the formulas:

$$\omega_\eta = \frac{2(A-1)}{\tau_0} \tag{35}$$

$$\omega_\psi = \frac{2(A-1)}{A\tau_0}. \tag{36}$$

The previously introduced TF represents a BP NGD function of passive topology when $A < 1$ and $\tau_0 < 0$. The magnitude given in equation (18) is transformed as:

$$T(\omega) = |T(j\omega)| = \frac{\sqrt{(\omega_0^2-\omega^2)^2+\omega_\eta^2\omega^2}}{\sqrt{(\omega_0^2-\omega^2)^2+\omega_\psi^2\omega^2}}. \tag{37}$$

The associated to TF transmission phase derived from equation (20) is given by:

$$\varphi(\omega) = \arctan\left(\frac{\omega_\eta\omega}{\omega_0^2-\omega^2}\right) - \arctan\left(\frac{\omega_\psi\omega}{\omega_0^2-\omega^2}\right). \tag{38}$$

The GD defined in equation (21) becomes:

$$GD(\omega) = \frac{(\omega_\psi-\omega_\eta)(\omega^2+\omega_0^2)}{\left[\omega^4-(\omega_\eta\omega_\psi+2\omega_0^2)\omega^2+\omega_0^4\right]}. \tag{39}$$
$$\left[\omega^4+(\omega_\eta^2-2\omega_0^2)\omega^2+\omega_0^4\right]$$
$$\left[\omega^4+(\omega_\psi^2-2\omega_0^2)\omega^2+\omega_0^4\right]$$

3) BP NGD CHARACTERIZATION

At the frequency, $\omega = \omega_0$, the GD expressed previously is simplified as:

$$GD(\omega_0) = \frac{2(\omega_\eta-\omega_\psi)}{\omega_\eta\omega_\psi}. \tag{40}$$

By taking into account the parameters defined in equations (24) and (39), this formula is reduced to:

$$GD(\omega_0) = \tau_0. \tag{41}$$

This last relation explains that if $\tau_0 < 0$, we have a BP NGD function. As demonstrated in [37], the NGD cut-off frequencies are the root of equation $GD(\omega) = 0$. By considering the GD expressed in equation (39), the NGD cut-off frequencies associated to the H-tree topology can be formulated as:

$$\omega_a = \sqrt{\omega_0^2 + \frac{\omega_\eta\omega_\psi - \sqrt{\omega_\eta\omega_\psi(4\omega_0^2+\omega_\eta\omega_\psi)}}{2}} \tag{42}$$

$$\omega_b = \sqrt{\omega_0^2 + \frac{\omega_\eta\omega_\psi + \sqrt{\omega_\eta\omega_\psi(4\omega_0^2+\omega_\eta\omega_\psi)}}{2}}. \tag{43}$$

Moreover, the TF given in equation (37) will be reduced to:

$$T(\omega=\omega_0) = A. \tag{44}$$

The feasibility of NGD circuit design with respect to NGD, insertion and reflection coefficient specifications must be verified. To materialize the feasibility of the developed TAN and NGD theory, an example of LC network based resistorless H-tree will be investigated in the next section.

IV. NGD ANALYTICAL STUDY OF THE LC-NETWORK BASED RESISTORLESS H-TREE

The BP NGD behavior of the resistorless H-tree is explored in the present section. The NGD analysis following the previously described methodology will be carried out based on BP NGD specifications. The canonical form of BP NGD transmission coefficient is introduced.

A. RELFECTION COEFFICIENTS

This subsection is focused on the NGD specific analytical investigation. The expressions of the S-parameters will be explored. The reflection and transmission coefficients corresponding to the previously established S-parameters can be established in function of Laplace variable, s. The reflection coefficients are given by:

$$S_1^1(s) = S_2^2(s) = \frac{N_{11}(s)}{D_{11}(s)} \tag{45}$$

$$S_3^3(s) = S_4^4(s) = \frac{N_{33}(s)}{D_{33}(s)} \tag{46}$$

with:

$$N_{11}(s) = s.\begin{pmatrix} C^2L^2R_0^2s^3 - C^2R_0^4s + 2C_0CL^2R_0^2s^3 + \\ 2CL^2R_0s^2 + 2CLR_0^2s - 2C_0CR_0^4s - \\ 2CR_0^3 + 2C_0L^2R_0s^2 + L^2s + \\ 2C_0LR_0^2s + 2LR_0 - 2C_0R_0^3 \end{pmatrix} \tag{47}$$

$$D_{11}(s) = D_{33}(s) = \left\{\begin{bmatrix} CLR_0s^2 + (L+CR_0^2)s + 2R_0 \end{bmatrix} \right\} \tag{48}$$
$$\left\{\begin{bmatrix} 2R_0 + R_0L(C+2C_0)s^2 \\ +(L+(C+2C_0)R_0^2)s \end{bmatrix}\right\}$$

$$N_{33}(s) = s\left\{\begin{bmatrix} 2R_0\left[L - R_0^2(C+C_0)\right] + \\ \left[L^2 - 2R_0^2L(C+C_0) - R_0^4C(C+2C_0)\right]s \\ -R_0LC(C+2C_0)(2R_0+Ls)s^2 \end{bmatrix}\right\} \tag{49}$$

B. TRANSMISSION COEFFICIENTS

The analytical expressions of the transmission coefficients are:

$$S_2^1(s) = S_1^2(s) = S_4^3(s) = S_3^4(s) = \frac{2C_0R_0^3s}{D_{21}(s)} \tag{50}$$

$$S_3^1(s) = S_1^3(s) = S_4^2(s) = S_2^4(s) = \frac{N_{31}(s)}{D_{31}(s)} \tag{51}$$

$$S_4^1(s) = S_1^4(s) = S_3^2(s) = S_2^3(s) = \frac{N_{41}(s)}{D_{41}(s)} \tag{52}$$

$$S_4^3(s) = S_3^4(s) = \frac{N_{43}(s)}{D_{43}(s)} \tag{53}$$

with:

$$N_{31}(s) = 2R_0\left\{\begin{bmatrix} R_0L(C+C_0)s^2 + \\ \left[L+R_0^2(C+C_0)\right]s + 2R_0 \end{bmatrix}\right\} \tag{54}$$

$$N_{41}(s) = 2R_0^2C_0s(R_0+Ls) \tag{55}$$

$$N_{23}(s) = 2R_0C_0s(R_0+Ls)^2 \tag{56}$$

$$D_{43}(s) = D_{41}(s) = D_{31}(s) = D_{21}(s) = D_{11}(s) \tag{57}$$

C. TRANSMISSION PHASE RESPONSE EXPRESSIONS

The transmission phases associated to the transmission coefficients in equations (50) to (53) are expressed as, respectively:

$$\varphi_1^2(\omega) = \frac{\pi}{2} - \varphi_0(\omega) \tag{58}$$

$$\varphi_1^3(\omega) = \arctan\left[\frac{(R_0^2C + L)\omega}{2R_0 - R_0L(C + C_0)\omega^2}\right] - \varphi_0(\omega) \tag{59}$$

$$\varphi_1^4(\omega) = \frac{\pi}{2} + \arctan\left(\frac{L\omega}{R_0}\right) - \varphi_0(\omega) \tag{60}$$

with:

$$\varphi_0(\omega) = \left\{\begin{array}{l}\arctan\left[\dfrac{(R_0^2C + L)\omega}{2R_0 - R_0LC\omega^2}\right] + \\ \arctan\left[\dfrac{\left[R_0^2(C + 2C_0) + L\right]\omega}{R_0\left[2 - L(C + 2C_0)\omega^2\right]}\right]\end{array}\right\}. \tag{61}$$

D. GD RESPONSE EXPRESSIONS

The GD associated to the signal propagating from port ❶ to ports ❷, ❸ and ❹ the resistorless H-tree can be written compactly as:

$$GD_1^2(\omega) = \frac{\partial\varphi_0(\omega)}{\partial\omega} \tag{62}$$

$$GD_1^3(\omega) = -\frac{\partial\varphi_1^3(\omega)}{\partial\omega} \tag{63}$$

$$GD_1^4(\omega) = -\frac{\partial\varphi_1^4(\omega)}{\partial\omega} \tag{64}$$

$$GD_3^4(\omega) = -\frac{\partial\varphi_3^4(\omega)}{\partial\omega}. \tag{65}$$

For the sake of mathematical complexity, the analytical expressions of these GDs will not be explored in the present section. However, an investigation on the transmission coefficient susceptible to generate the BP NGD function will be proposed in the next subsection.

E. IDENTIFICATION OF CANONICAL FORM

By identification of the adequate transmission coefficient with the TF canonical form introduced in equation (34), we can forecast the BP NGD function. Among the different transmission coefficients, we can expect the canonical formula from the following decomposition:

$$S_1^3(s) = T(s) \cdot T_0(s) \tag{66}$$

with:

$$T(s) = \frac{\begin{array}{c}R_0L(C + C_0)s^2 + \\ \left[L + R_0^2(C + C_0)\right]s + 2R_0\end{array}}{\begin{array}{c}2R_0 + R_0L(C + 2C_0)s^2 \\ +(L + (C + 2C_0)R_0^2)s\end{array}} \tag{67}$$

$$T_0(s) = \frac{\frac{2R_0C + C_0)}{(C + 2C_0)}}{CLR_0s^2 + (L + CR_0^2)s + 2R_0} \tag{68}$$

The first quantity can be identified by the characteristic parameters:

$$\omega_\eta = \frac{L + R_0^2(C + C_0)}{R_0L(C + C_0)} \tag{69}$$

$$\omega_\psi = \frac{L + (C + 2C_0)R_0^2}{R_0L(C + 2C_0)}. \tag{70}$$

We can assume the other last canonical form parameters as:

$$\omega_0 = \frac{2R_0}{R_0L(C + C_0)}. \tag{71}$$

At this frequency, the H-tree GD given in equation (40) becomes:

$$GD(\omega_0) = \frac{2R_0^3LC_0(C + 2C_0)}{\left[L + R_0^2(C + C_0)\right]\left[L + R_0^2(C + 2C_0)\right]}. \tag{72}$$

To verify the BP NGD analysis feasibility, simulation and experimental results will be presented in the next subsection.

V. DISCUSSION ON CALCULATED, SIMULATED AND EXPERIMENTED RESULTS

The relevance of the TAN NGD theory established in the previous section is verified in the present one. A POC of resistorless H-tree circuit will be considered for the validation study. The modelling will be based on the calculation with MATLAB® implementation of the previously established S-parameters, phases, and GDs in equations (25), (26) and (27), respectively. Then, the results will be compared with simulations and measurements. The simulations are performed in the schematic environment of the electronic circuit designer and simulator ADS® from Keysight Technologies®.

A. DESCRIPTION OF THE RESISTORLESS H-TREE POC PROTOTYPES

The POC schematic of the resistorless H-tree circuit is presented in Fig. 5(a). The POC circuit schematic was parametrized with arbitrary chosen values in order to demonstrate the feasibility of the BP NGD function. The H-tree circuit was designed and fabricated with lumped L and C components. The photograph of the tested prototype is displayed by Fig. 5(b). The PCB is implemented on Cu-metalized FR4 dielectric substrate in hybrid technology. It is noteworthy that in difference to the existing NGD circuits [12]–[16], we emphasize that this H-circuit prototype is originally designed as a four-port PCB which is only constituted by reactive components with no resistive element. The parameters of POC constituting the fabricated H-tree PCB prototype are indicated in Table 2.

The following subsection examines the obtained validation results.

B. DISCUSSION ON THE BP NGD VALIDATION RESULTS

By using the modelled, simulated and fabricated POC prototype, we studied the results of the tests. Different verifications with the resistorless and symmetric LC-network H-tree topology is investigated in the present subsection. The BP NGD

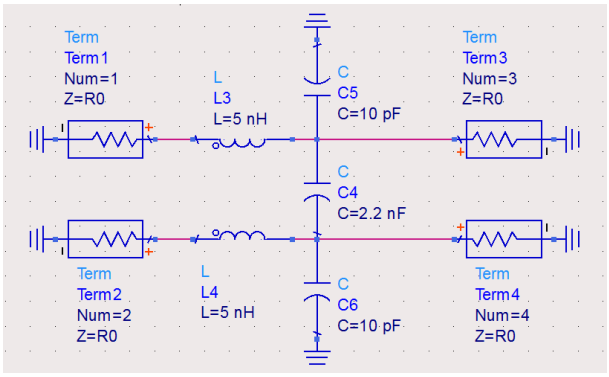

(a)

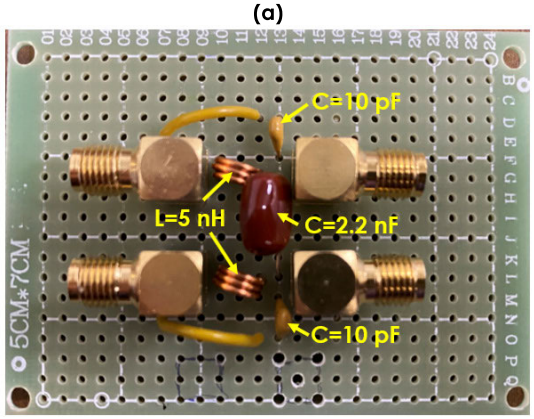

(b)

FIGURE 5. (a) Schematic and (b) photograph of the resistorless H-tree prototype.

TABLE 2. Parameters of the components constituting the H-Tree PCB prototype.

Type	Construction technology	Nominal value	Tolerance
Inductor	Copper coilcraft	L=10 nH	+/- 3%
Capacitor	Tantalum	C=10 pF	+/- 1%
	Silver mica	C_0=2.2 nF	+/- 1%

function validation is discussed after the description of the experimental setup.

1) EXPERIMENTAL SETUP DESCRIPTION

Similar to the classical RF and microwave circuits, the NGD tests of the H-tree circuit proposed in Figs. 6 were carried out based on the four-port S-parameter analysis. The measurement was done with a Vector Network Analyzer (VNA) as illustrated by the experimental setup shown in the photograph of Figs. 5. The employed four-port VNA is referenced ENA Series E5071C from Keysight Technologies® which has frequency band delimited from 9 kHz to 8.5 GHz. The S-parameter measurement test was made under SOLT calibration.

The next paragraphs are focused on the results of the reflection and transmission coefficients added with the GD comparisons.

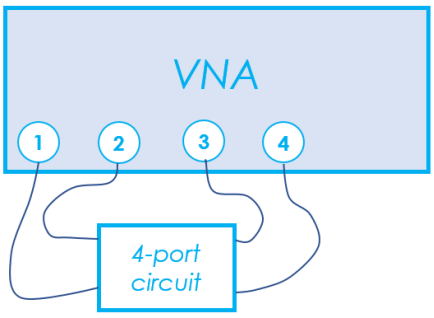

(a)

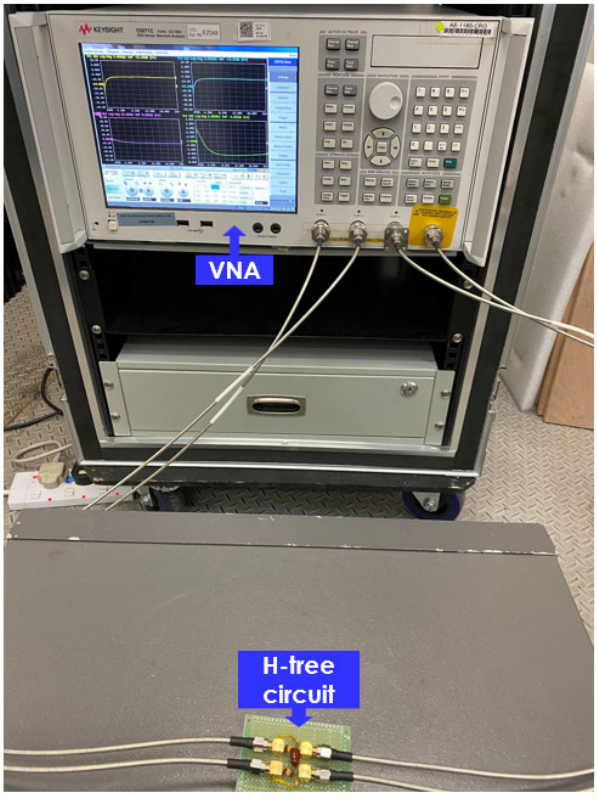

(b)

FIGURE 6. Configuration of the resistorless H-tree prototype experimental setup.

2) REFLECTION S-PARAMETER RESULTS

Comparisons of the simulated (“Sim.”), measured (“Meas.”) and calculated (“Calc.”) reflection coefficient results, $S_1^1 = S_2^2$ and $S_3^3 = S_4^4$, of the H-tree circuit POC are examined in the present paragraph. The different responses are displayed in blue solid, black dashed and red dotted curves of Figs. 7. The validation S-parameter analyses were presented in the frequency band from 50 kHz to 27 MHz. The corresponding results of $S_1^1 = S_2^2$ and $S_3^3 = S_4^4$, are plotted in Fig. 7(a) and in Fig. 7(b), respectively. We can emphasize that the H-tree POC TAN calculated reflection coefficients are in very good correlation with the simulation and measured result in the considered frequency band of the study. The slight differences of less than 0.5 dB mainly due to the tolerances and the parasitic effects of the used components.

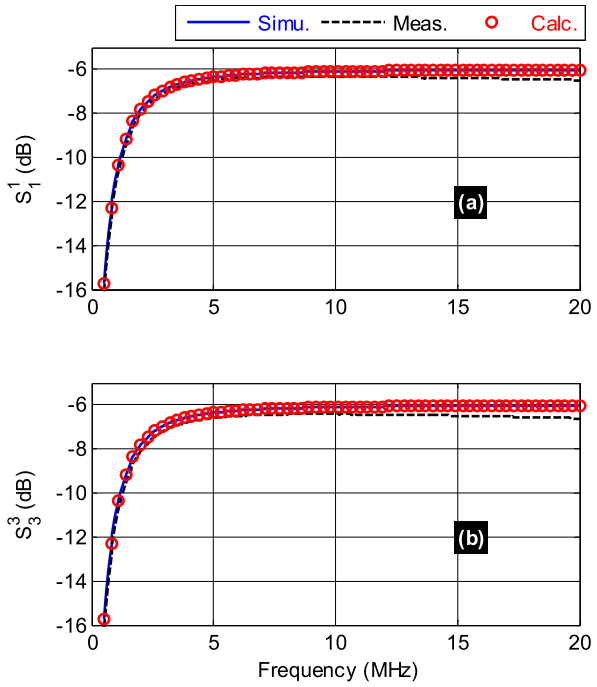

FIGURE 7. Comparisons between simulated, measured and calculated reflection coefficients of the H-tree circuit prototype: (a) $S_1^1 = S_2^2$ and (b) $S_3^3 = S_4^4$.

To complete the S-parameter verification, we will also compare in the following paragraph the transmission coefficients between the different ports of the H-tree circuit.

3) TRANSMISSION S-PARAMETER RESULTS

Fig. 8(a) and Fig. 8(b) show the plots of the transmission coefficients, S_1^2 and S_1^3, of the tested H-tree prototype, respectively. In addition, the transmission parameters through the other ports, S_1^4 and S_3^4, are also displayed in Fig. 9(a) and in Fig. 9(b). As expected, a good agreement between the transmission parameters are observed in the considered frequency range. These results confirm the effectiveness of the TAN modelling for predicting the S-parameter responses of the H-tree topology.

To verify the BP NGD behavior, the GD responses were also compared in the following paragraph.

4) GD RESULTS

The simulated, measured and calculated GDs expressed in equations (50), (51), (52) and (53), of the H-tree circuit prototype were plotted. Those associated to transmission coefficients, S_1^2, S_1^4 and S_3^4 are displayed in Fig. 10(a), Fig. 10(b) and Fig. 10(c), respectively. It can be pointed out that these comparative results present a very good agreement. However, the GDs are all having positive values from 50 kHz to 27 MHz. However, the comparative plots of simulated, measured and calculated GDs displayed in Fig. 10 confirm the observation of the BP NGD aspect. We can characterize the simulated and calculated BP NGD responses with NGD center frequency of approximately $f_0 = 3.6$ MHz and GD

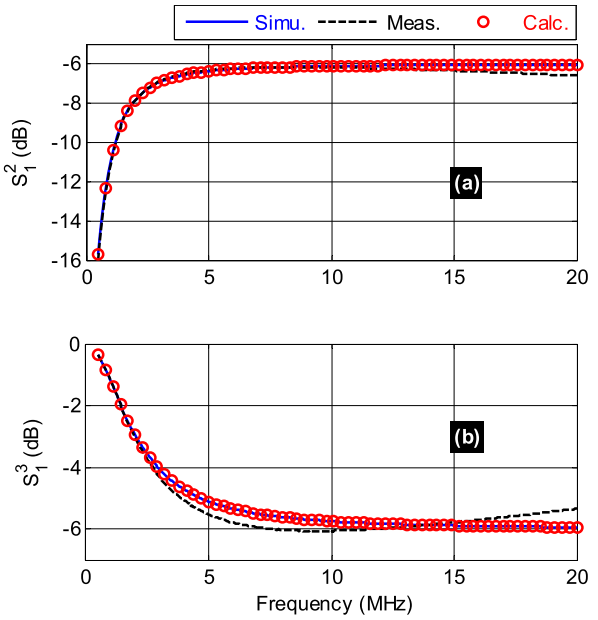

FIGURE 8. Comparisons between simulated, measured and calculated transmission coefficients of the H-tree circuit prototype: (a) $S_{21} = S_{43}$ and (b) $S_{31} = S_{42}$.

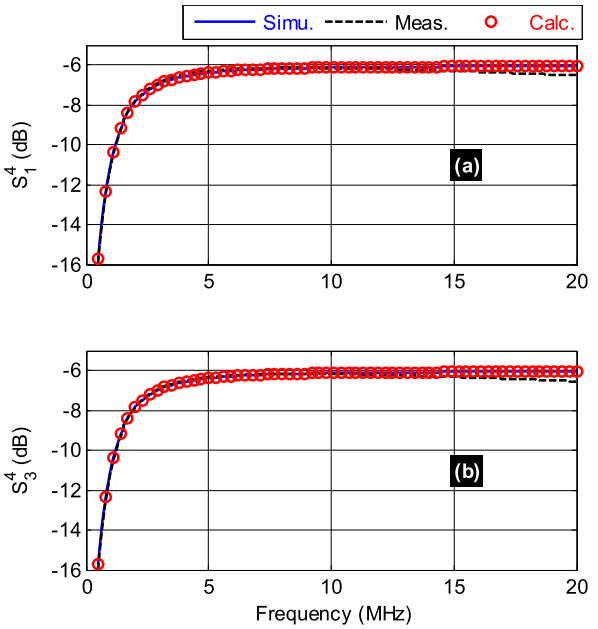

FIGURE 9. Comparisons between simulated, measured and calculated transmission coefficients of the H-tree circuit prototype: (a) $S_1^4 = S_2^3$ and (b) $S_4^3 = S_3^4$.

value of about $GD_0 = -6$ ns. Nevertheless, we have fluctuation of the measured results compared to the simulated and calculated ones. The imperfections of the experimental results can be explained by the VNA measurement noises which are more significant when the operating frequency is lower than 50 MHz.

The overall results of calculations, simulations and measurements uphold that the BP NGD function can be

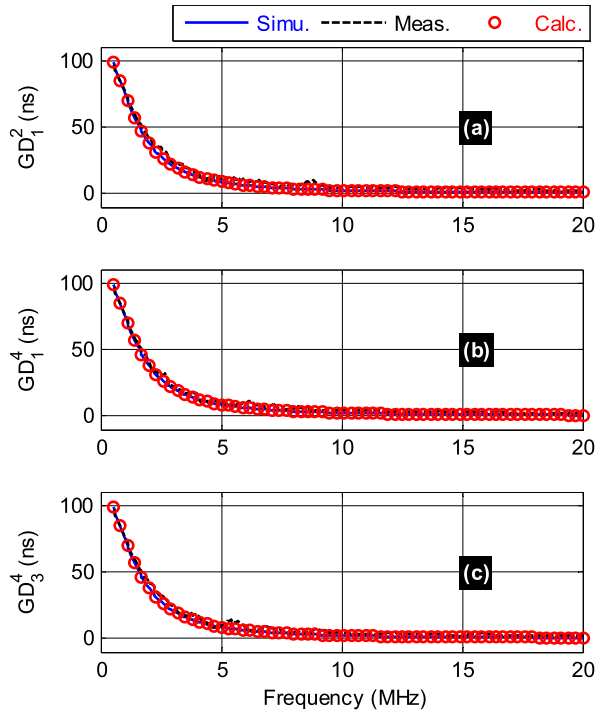

FIGURE 10. Comparisons between simulated, measured and calculated GDs from transmission coefficients, (a) S_1^2, (a) S_1^4 and (a) S_3^4 of the H-tree circuit prototype.

TABLE 3. Comparison of BP NGD specifications from the GD associated to transmission coefficient S_1^3.

Approach	f_o	$GD(f_o)$	BW	$S_{21}(f_o)$	$S_{11}(f_o)$
Calc.	3.6 MHz	-6 ns	22.8 MHz	-6.68 dB	-6.65 dB
Simu.	3.58 MHz	-6.01 ns	22.9 MHz	-6.7 dB	-6.64 dB
Meas.	3.7 MHz	-8.5 ns	18.7 MHz	-6.9 dB	-6.79 dB

implemented with resistorless and symmetrical H-tree circuit introduced in Figs. 5.

5) DISCUSSION ON THE CALCULATED, SIMULATED AND MEASURED NGD PERFORMANCES

The previous BP NGD validation of the resistorless and symmetric LC-network H-tree topology leads to the discussion on the parameters. Table 3 addresses the different values of the simulated, calculated and measured NGD parameters. We can point out that the attenuation loss is close to 6.6 dB around the NGD center frequency. But the reflection losses are slightly less than 7 dB.

In the next step of the study, the optimization technique of the four-port NGD circuit will be developed in order to ensure the BP NGD function with respect to the constraints between the reflection and transmission losses.

C. SENSIVITY STUDY OF L AND C COMPONENT VARIATIONS

The robustness of the BP NGD function with the resistorless H-tree with respect to the +/−5% relative variation of each component nominal value was studied. The following paragraphs described the obtained results with the mappings of the GD and S-parameters, S_1^1, S_1^3 and S_3^3 related to the connection between port 1 and port 3 where we have the NGD behavior.

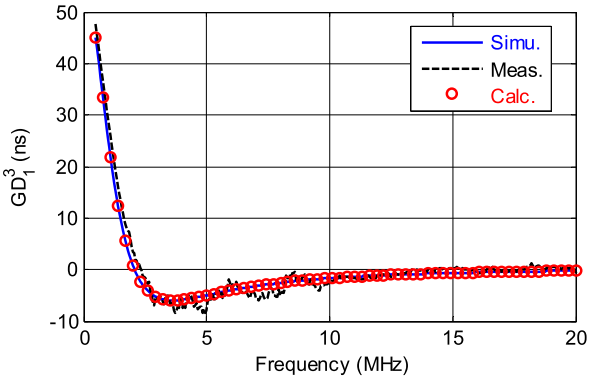

FIGURE 11. Comparisons between simulated, measured and calculated GDs from transmission coefficient, S_1^3 of the H-tree circuit prototype.

1) INFLUENCE OF L

Fig. 12 shows the mapping of the GD versus the couple of variables (f, L) by varying only one of the inductance in the arm of the resistorless H-tree. The frequency x-axis is presented in logarithmic scale for the better presentation in the considered range of the frequency. During this sensitivity analysis (SA), the inductance was linearly varied from $L_{min} = 5.225$ nH and $L_{max} = 5.775$ nH. We can see that the BP NGD behavior is conserved in the range of +/−5% variation of the inductance.

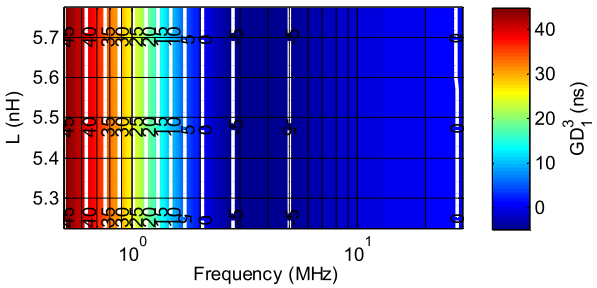

FIGURE 12. Mapping of GD related transmission coefficient, S_1^3 versus (f, L).

Furthermore, the associated reflection and transmission coefficients are mapped in Figs. 13 in semi-logarithmic scale like for the GD. We can see an absolute variation of the magnitudes of S-parameters less than 1 dB.

2) INFLUENCE OF C

As a second SA, Fig. 14 shows the mapping of the H-tree GD versus the couple of variables (f, C). The frequency xaxis is presented in logarithmic scale. In this case, the one of lateral capacitor of the H-tree was linearly varied from $C_{min} = 9.5$ pF and $C_{max} = 10.5$ pF. Hence, the cartographies of the associated S-parameters are displayed in Figs. 15. It can be understood with all the mappings, the variations of the BP

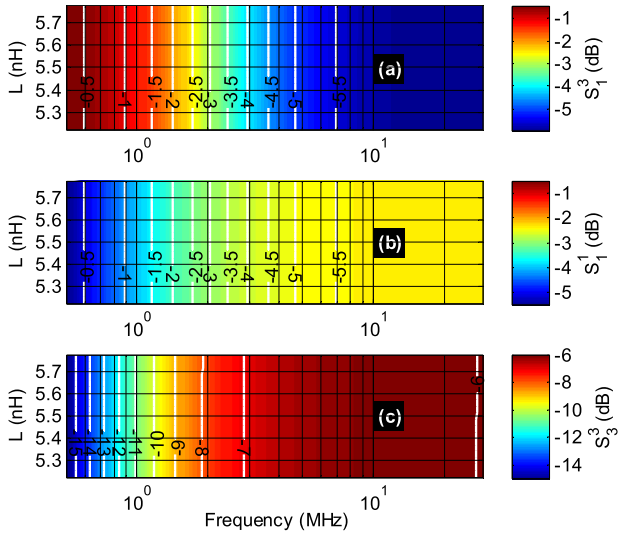

FIGURE 13. Mappings of (a) S_1^3, (b) S_1^1 and (c) S_3^3 magnitudes versus (f, L).

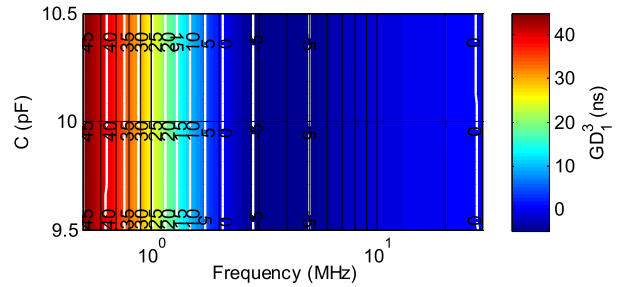

FIGURE 14. Mapping of GD related transmission coefficient, S_1^3 versus (f, C).

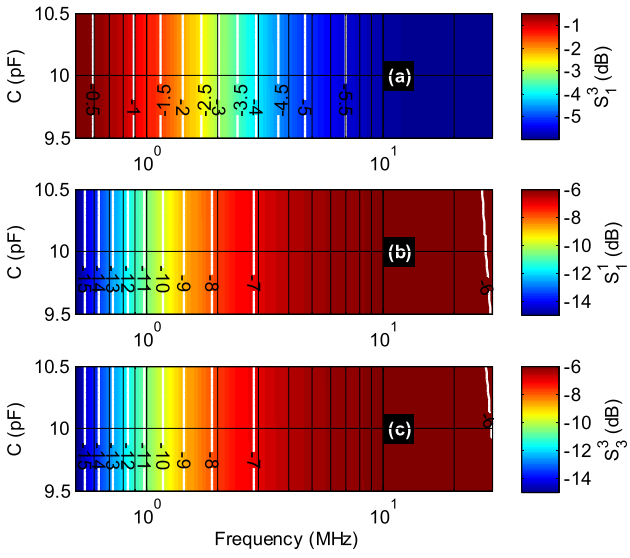

FIGURE 15. Mappings of (a) S_1^3, (b) S_1^1 and (c) S_3^3 magnitudes versus (f, C).

NGD parameters are not significant with respect to the SA of C.

3) INFLUENCE OF C_0

In this last case of SA, the influence of C_0 is studied. Fig. 16 depicts the influence to the GD response versus

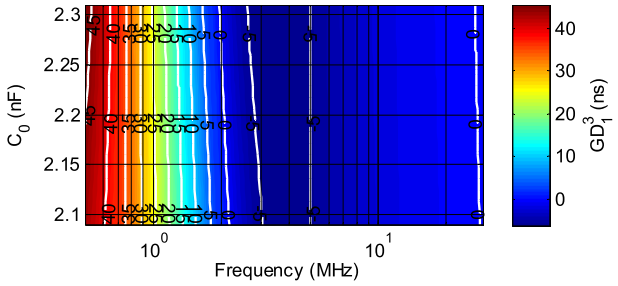

FIGURE 16. Mapping of GD related transmission coefficient, S_1^3 versus (f, C_0).

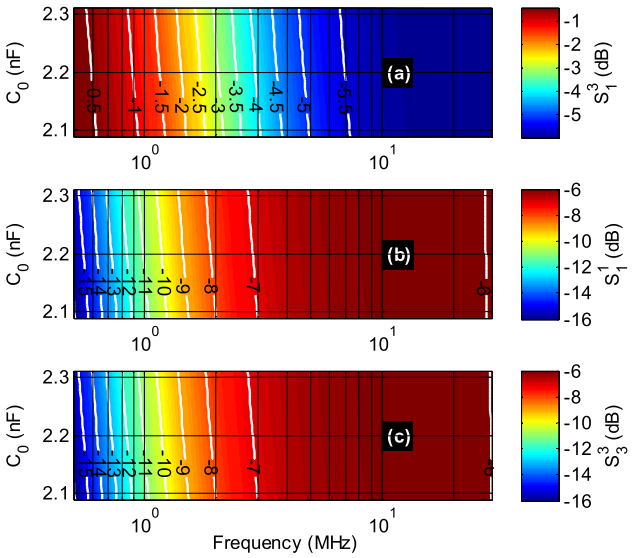

FIGURE 17. Mappings of (a) S_1^3, (b) S_1^1 and (c) S_3^3 magnitudes versus (f, C_0).

the couple of variables (f, C_0). In this study, the coupling capacitor was linearly varied from $C_{0\,min} = 2.09$ nF and $C_{0\,max} = 2.31$ nF.

We can point out from the cartography of Fig. 16 that this coupling capacitor variation changes slightly the NGD cut-off frequencies. The corresponding S-parameters are shown in Figs. 17. We can see that the variations of the transmission and reflection coefficients are not significant with the +/−5% relative variation of C_0.

VI. CONCLUSION

An innovative BP NGD analysis of a four-port symmetric lumped circuit is investigated. The considered four-port topology is constituted by resistorless and symmetric H-tree using LC-passive network. The multi-port topology theory is established by the S-parameter modelling. The analytical model was determined based on the TAN formalism. The methodology of the BP NGD analysis is described with all the analytical expressions constituting the different steps.

The feasibility study of the BP NGD behavior is verified with an H-tree circuit prototype. The resistorless H-tree POC is implemented with commercial components. The S-parameter results from analytical calculation, simu-

lation and measurement are compared. The simulation was performed with a commercial tool and the measurement was generated from the VNA test. As expected, a very good agreement between the reflection and transmission coefficients through the different ports of the H-tree circuit is observed. Then, the BP NGD analysis is validated with the GD response between port 1 and port 3 of the H-tree circuit prototype.

The proposed resistorless BP NGD topology is potentially useful to avoid the attenuation loss induced by the resistor component. As proposed in [38]–[40], the main applications NGD circuit is the equalization of signal delay or the correction of the signal synchronization in multi-port electronic sensors. An example of sensor signal prediction from mechanical actions which can be extended to megahertz frequency range is demonstrated in reference [40].

REFERENCES

[1] S.-S. Myoung, B.-S. Kwon, Y.-H. Kim, and J.-G. Yook, "Effect of group delay in RF BPF on impulse radio systems," *IEICE Trans. Commun.*, vol. E90-B, no. 12, pp. 3514–3522, Dec. 2007.

[2] B. Nikfal, S. Gupta, and C. Caloz, "Increased group-delay slope loop system for enhanced-resolution analog signal processing," *IEEE Trans. Microw. Theory Techn.*, vol. 59, no. 6, pp. 1622–1628, Jun. 2011.

[3] K.-P. Ahn, R. Ishikawa, and K. Honjo, "Group delay equalized UWB InGaP/GaAs HBT MMIC amplifier using negative group delay circuits," *IEEE Trans. Microw. Theory Techn.*, vol. 57, no. 9, pp. 2139–2147, Sep. 2009.

[4] B. Ravelo, S. Lalléchère, A. Thakur, A. Saini, and P. Thakur, "Theory and circuit modeling of baseband and modulated signal delay compensations with low- and band-pass NGD effects," *AEU-Int. J. Electron. Commun.*, vol. 70, no. 9, pp. 1122–1127, Sep. 2016.

[5] M. W. Mitchell and R. Y. Chiao, "Negative group delay and 'fronts' in a causal system: An experiment with very low frequency bandpass amplifiers," *Phys. Lett. A*, vol. 230, nos. 3–4, pp. 133–138, Jun. 1997.

[6] M. Kitano, T. Nakanishi, and K. Sugiyama, "Negative group delay and superluminal propagation: An electronic circuit approach," *IEEE J. Sel. Topics Quantum Electron.*, vol. 9, no. 1, pp. 43–51, Jan. 2003.

[7] J. N. Munday and R. H. Henderson, "Superluminal time advance of a complex audio signal," *Appl. Phys. Lett.*, vol. 85, no. 3, pp. 503–505, Jul. 2004.

[8] J. N. Munday and W. M. Robertson, "Observation of negative group delays within a coaxial photonic crystal using an impulse response method," *Opt. Commun.*, vol. 273, no. 1, pp. 32–36, May 2007.

[9] O. F. Siddiqui, S. J. Erickson, G. V. Eleftheriades, and M. Mojahedi, "Time-domain measurement of negative group delay in negative-refractive-index transmission-line metamaterials," *IEEE Trans. Microw. Theory Techn.*, vol. 52, no. 5, pp. 1449–1454, May 2004.

[10] F. Wan, N. Li, B. Ravelo, J. Ge, and B. Li, "Time-domain experimentation of NGD ActiveRC-network cell," *IEEE Trans. Circuits Syst. II, Exp. Briefs*, vol. 66, no. 4, pp. 562–566, Apr. 2019.

[11] H. Mao, L. Ye, and L.-G. Wang, "High fidelity of electric pulses in normal and anomalous cascaded electronic circuit systems," *Results Phys.*, vol. 13, no. 102348, pp. 1–9, Jun. 2019.

[12] C. D. Broomfield and J. K. A. Everard, "Broadband negative group delay networks for compensation of microwave oscillators and filters," *Electron. Lett.*, vol. 36, no. 23, pp. 1931–1933, Nov. 2000.

[13] K.-P. Ahn, R. Ishikawa, A. Saitou, and K. Honjo, "Synthesis for negative group delay circuits using distributed and second-order RC circuit configurations," *IEICE Trans. Electron.*, vol. E92-C, no. 9, pp. 1176–1181, 2009.

[14] G. V. Eleftheriades, O. Siddiqui, and A. K. Iyer, "Transmission line models for negative refractive index media and associated implementations without excess resonators," *IEEE Microw. Wireless Compon. Lett.*, vol. 13, no. 2, pp. 51–53, Feb. 2003.

[15] O. F. Siddiqui, M. Mojahedi, and G. V. Eleftheriades, "Periodically loaded transmission line with effective negative refractive index and negative group velocity," *IEEE Trans. Antennas Propag.*, vol. 51, no. 10, pp. 2619–2625, Oct. 2003.

[16] M. Kandic and G. E. Bridges, "Asymptotic limits of negative group delay in active resonator-based distributed circuits," *IEEE Trans. Circuits Syst. I, Reg. Papers*, vol. 58, no. 8, pp. 1727–1735, Aug. 2011.

[17] B. Ravelo, "Similitude between the NGD function and filter gain behaviours," *Int. J. Circuit Theory Appl.*, vol. 42, no. 10, pp. 1016–1032, Oct. 2014.

[18] Y. Awatsuji and T. Kubota, "Two-dimensional H-tree parallel optical interconnect for two-dimensional image by using optical iterative processing," *IEEE Photon. Technol. Lett.*, vol. 13, no. 1, pp. 79–81, Jan. 2001.

[19] Y. Yamada, H. Amano, M. Koibuchi, A. Jouraku, K. Anjo, and K. Nishimura, "Folded fat H-tree: An interconnection topology for dynamically reconfigurable processor array," in *Embedded and Ubiquitous Computing* (Lecture Notes in Computer Science), vol. 3207, L. T. Yang, M. Guo, G. R. Gao, and N. K. Jha, Eds. Berlin, Germany: Springer, 2004, pp. 301–311.

[20] M. A. El-Moursy and E. G. Friedman, "Exponentially tapered H-tree clock distribution networks," *IEEE Trans. Very Large Scale Integr. (VLSI) Syst.*, vol. 13, no. 8, pp. 971–975, Aug. 2005.

[21] J. Rosenfeld and E. G. Friedman, "Design methodology for global resonant H-tree clock distribution networks," *IEEE Trans. Very Large Scale Integr. (VLSI) Syst.*, vol. 15, no. 2, pp. 135–148, Feb. 2007.

[22] I. Chanodia and D. Velenis, "Parameter variations and crosstalk noise effects on high performance H-tree clock distribution networks," *Anal. Integr. Circuits Signal Process.*, vol. 56, nos. 1–2, pp. 13–21, Aug. 2008.

[23] W.-K. Loo, K.-S. Tan, and Y.-K. Teh, "A study and design of CMOS H-tree clock distribution network in system-on-chip," in *Proc. 8th IEEE Int. Conf. ASIC*, Changsha, China, Oct. 2009, pp. 411–414.

[24] T. Eudes and B. Ravelo, "Analysis of multi-gigabits signal integrity through clock H-tree: Analysis of multi-gigabits signal integrity through clock H-tree," *Int. J. Circuit Theory Appl.*, vol. 41, no. 5, pp. 535–549, May 2013.

[25] H. Lu, C. Su, and C.-N. Jimmy Liu, "A tree-topology multiplexer for multiphase clock system," *IEEE Trans. Circuits Syst. I, Reg. Papers*, vol. 56, no. 1, pp. 124–131, Jan. 2009.

[26] N. Rakuljic and I. Galton, "Tree-structured DEM DACs with arbitrary numbers of levels," *IEEE Trans. Circuits Syst. I, Reg. Papers*, vol. 57, no. 2, pp. 313–322, Feb. 2010.

[27] N. Jain, V. Prasad, and A. Bhattacharyya, "Delay-time sensitivity in linear RC tree," *IEEE Trans. Circuits Syst.*, vol. 34, no. 4, pp. 443–445, Apr. 1987.

[28] C.-W. A. Tsao and C.-K. Koh, "A clock tree router for general skew constraints," *J. ACM TODAES*, vol. 7, no. 3, pp. 359–379, 2002.

[29] Z. Xu, B. Ravelo, O. Maurice, S. Lalléchère, and F. Wan, "Kron-branin modeling of symmetric star tree interconnect," *Int. J. Circuit Theory Appl.*, vol. 47, no. 3, pp. 391–405, Mar. 2019.

[30] G. Kron, *Tensor Analysis of Networks*. New York, NY, USA: Wiley, 1939.

[31] O. Maurice, *Elements of Theory for Electromagnetic Compatibility and Systems*. Aix-en-Provence, France: Bookelis, 2017.

[32] O. Maurice, A. Reineix, P. Hoffmann, B. Pecqueux, and P. Pouliguen, "A formalism to compute the electromagnetic compatibility of complex networks," *Adv. Appl. Sci. Res.*, vol. 2, no. 5, pp. 439–448, 2011.

[33] O. Maurice, A. Reineix, P. Durand, and F. Dubois, "On mathematical definition of chords between networks," in *Proc. Eur. Electromagn. (EuroEM)*, Toulouse, France, Jul. 2012, pp. 1–3.

[34] P. Durand, O. Maurice, and A. Reineix, "Generalized interaction principle implemented in the Kron's method," in *Proc. World Congr. Eng. (WCE)*, London, U.K., vol. 1, Jul. 2013, pp. 1–4.

[35] O. Maurice, A. Reineix, P. Durand, and F. Dubois, "Kron's method and cell complexes for magnetomotive and electromotive forces," *Int. J. Appl. Math.*, vol. 44, no. 4, pp. 183–191, 2014.

[36] C. Cholachue, B. Ravelo, A. Simoens, and A. Fathallah, "Fast S-parameter TAN model of n-port lumped structures," *IEEE Access*, vol. 7, pp. 72505–72517, Dec. 2019.

[37] B. Ravelo, S. Ngoho, G. Fontgalland, L. Rajaoarisoa, W. Rahajandraibe, R. Vauche, Z. Xu, F. Wan, J. Ge, and S. Lallechere, "Original theory of NGD low pass-high pass composite function for designing inductorless BP NGD lumped circuit," *IEEE Access*, vol. 8, pp. 192951–192964, Oct. 2020.

[38] F. Wan, X. Miao, B. Ravelo, Q. Yuan, J. Cheng, Q. Ji, and J. Ge, "Design of multi-scale negative group delay circuit for sensors signal time-delay cancellation," *IEEE Sensors J.*, vol. 19, no. 19, pp. 8951–8962, Oct. 2019.

[39] F. Wan, Z. Yuan, B. Ravelo, J. Ge, and W. Rahajandraibe, "Low-pass NGD voice signal sensoring with passive circuit," *IEEE Sensors J.*, vol. 20, no. 12, pp. 6762–6775, Jun. 2020.

[40] B. Ravelo, F. Wan, and J. Ge, "Anticipating actuator arbitrary action with a low-pass negative group delay function," *IEEE Trans. Ind. Electron.*, vol. 68, no. 1, pp. 694–702, Jan. 2021.

BLAISE RAVELO (Member, IEEE) is currently a University Full Professor with NUIST, Nanjing, China. He is a pioneer of the negative group delay (NGD) concept about t<0 signal travelling physical space. This extraordinary concept is potentially useful for anticipating and prediction all kind of information. He is a Lecturer on circuit and system theory, science, technology, engineering and maths (STEM), and applied physics. He was a Research Director of 11 Ph.D. students (eight defended), postdoctors, research engineers, and master internships. With USA, Chinese, Indian, European, and African partners, he is actively involved and contributes on several international research projects (ANR, FUI, FP7, INTERREG, H2020, Euripides^2, Eurostars...). He is the coauthor of more than 350 scientific research papers in new technologies published in international conferences and journals. His Google scholar h-index in 2021 is 22 and his i10 index is 59. His research interest includes multiphysics and electronics engineering. He is a member of IET Electronics Letters. He is an editorial board as a circuit and system subject editor. Since 2013, he has been a member of scientific technical committee of Advanced Electromagnetic Symposium (AES). He is a member of research groups, such as IEEE, URSI, GDR Ondes, Radio Society. He is regularly invited to review articles submitted for publication to international journals, such as the IEEE TRANSACTIONS ON MICROWAVE THEORY AND TECHNIQUES, the IEEE TRANSACTIONS ON CIRCUITS AND SYSTEMS, the IEEE TRANSACTIONS ON ELECTROMAGNETIC COMPATIBILITY, the IEEE TRANSACTIONS ON INDUSTRIAL ELECTRONICS, IEEE ACCESS, *IET CDS*, *IET MAP*, and so on, and books (Wiley, Intech Science, and so on).

FAYU WAN (Member, IEEE) received the Ph.D. degree in electronic engineering from the University of Rouen, Rouen, France, in 2011. From 2011 to 2013, he was a Postdoctoral Fellow with the Electromagnetic Compatibility Laboratory, Missouri University of Science and Technology, Rolla. He is currently a Full Professor with the Nanjing University of Information Science and Technology, Nanjing, China. His current research interests include negative group delay circuits, electrostatic discharge, electromagnetic compatibility, and advanced RF measurement.

JAMEL NEBHEN (Member, IEEE) received the M.Sc. degree in microelectronics from the National Engineering School of Sfax, Tunisia, in 2007, and the Ph.D. degree in microelectronics from Aix-Marseille University, France, in 2012. From 2012 to 2018, he worked as a Postdoctoral Researcher in France in LIRMM-Lab Montpellier, IM2NP-Lab Marseille, ISEP Paris, LE2I-Lab Dijon, Lab-Sticc Telecom Bretagne Brest, and IEMN-Lab Lille. Since 2019, he has been as an Assistant Professor with Prince Sattam bin Abdulaziz University, Alkharj, Saudi Arabia. His research interests include design of analog and RF integrated circuits, the IoT, biomedical circuit, and sensors instrumentation.

GEORGE CHAN (Senior Member, IEEE) received the B.Eng. degree (Hons.) in electronic and communication engineering from the City University of Hong Kong, and the M.Sc. degree in electronic and information engineering from The Hong Kong Polytechnic University.

He is currently a Senior Product Safety Engineer with ASM Pacific Technology Ltd. He has coauthored several technical publications in international journals and conference proceedings. His research interests include electromagnetic safety, EMC measurement, and EMC management. He is a member of the IEEE EMC Society TC1 on EMC Management. He is also a member of the IEEE International Committee for Electromagnetic Safety (ICES) Standards Coordinating Committee (SCC39) and a TC95 Sub-committee Member. He is an International Electrotechnical Commission (IEC) expert and a Committee Member of IEC TC106/PT63184 on Method for the assessment of electric, magnetic and electromagnetic fields associated with human exposure.

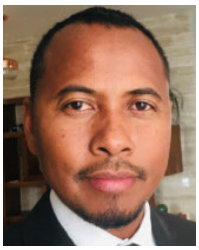

WENCESLAS RAHAJANDRAIBE (Member, IEEE) received the B.Sc. degree in electrical engineering from Nice Sophia-Antipolis University, France, in 1996, the M.Sc. degree (Hons.) in electrical engineering from the Science Department, University of Montpellier, France, in 1998, and the Ph.D. degree in microelectronics from the University of Montpellier. Since 1998, he has been with the Informatics, Robotics and Microelectronics Laboratory of Montpellier (LIRMM), Microelectronics Department. Since 2003, he has been with the Microelectronic Department, Institute of Materials, Microelectronics and Nanoscience Laboratory of Provence (IM2NP), Marseille, France, where he was an Associate Professor. Since 2014, he has been a Professor with Aix Marseille University where he heads the Integrated Circuit Design Group, IM2NP Laboratory. He is currently a Full Professor with the University of Aix-Marseille. He is regularly involved to participate and to lead national and international research projects, such as ANR, H2020, FP7 KIC-InnoEnergy, and so on. He directed and co-supervised 18 Ph.D. and 15 Master students. He is the author or coauthor of 11 patents and more than 150 papers published in refereed journals and conferences. His research interests include AMS and RF circuit design from transistor to architectural level, ultralow power circuit design for smart sensor interface and embedded electronic in bioelectronic and e-health applications, wireless systems, and design technique and architecture for multi-standard transceiver. He is an expert for the ANR, the French Agency for Research. He has served on program committees for IEEE NEWCAS and ICECS. He has been and is a Reviewer of contributions submitted to several IEEE conferences and journals, such as ISCAS, NEWCAS, MWSCAS, ESSCIRC, ESSDERC, RFIC, the IEEE TRANSACTIONS ON CIRCUITS AND SYSTEMS I AND II, and *IET Electronics Letters*.

SÉBASTIEN LALLÉCHÈRE (Member, IEEE) was born in Nevers, France, in 1979. He received the M.Sc. degree in computational modeling and electronics/electromagnetism from Polytech Clermont, in 2002, and the Ph.D. degree in computational modeling and electronics/electromagnetism from the Universite Blaise Pascal, Clermont-Ferrand, France, in 2006.

He worked as a Research Engineer with LASMEA, Clermont-Ferrand, in 2007, focusing on intensive computational methods for electromagnetics. He is currently an Associate Professor with the Institut Pascal and Universite Clermont Auvergne, Clermont-Ferrand, France. His research interests include electromagnetic compatibility including antennas and propagation, complex and reverberating electromagnetic environments, electromagnetic coupling, computational electromagnetics, stochastic modeling, and sensitivity analysis in electrical engineering.